

article

”

empty empty itleempty

ABSTRACT

This study investigates regional space weather phenomena in central Mexico by isolating local geomagnetic responses from their planetary counterparts. Through the analysis of 20 intense geomagnetic storms, we discerned the ionospheric contributions within regional geomagnetic data recorded in central Mexico. Our findings underscore the predominant role of ionospheric disturbances in driving local geomagnetic responses. Notably, the *Disturbed Polar Current Number 2* and the *Disturbed Dynamo Current* emerged as particularly influential factors in regional geomagnetic activity. Importantly, our research establishes that regional geomagnetic responses can be accurately approximated by considering the combined impacts of planetary geomagnetic responses and the magnetic perturbations prompted by the aforementioned ionospheric currents.

empty empty itletempty

 ccastellanos@igeofisica.unam.mx (C.C. I.);
p.coronaromero@igeofisica.unam.mx (C. P.); americoo@igeofisica.unam.mx
(G.J. A.)
ORCID(s): 0000-0001-8818-5318 (C.C. I.); 0000-0002-2573-2967 (C. P.);
0000-0003-4774-1829 (G.J. A.)

ABSTRACT

This study investigates regional space weather phenomena in central Mexico by isolating local geomagnetic responses from their planetary counterparts. Through the analysis of 20 intense geomagnetic storms, we discerned the ionospheric contributions within regional geomagnetic data recorded in central Mexico. Our findings underscore the predominant role of ionospheric disturbances in driving local geomagnetic responses. Notably, the *Disturbed Polar Current Number 2* and the *Disturbed Dynamo Current* emerged as particularly influential factors in regional geomagnetic activity. Importantly, our research establishes that regional geomagnetic responses can be accurately approximated by considering the combined impacts of planetary geomagnetic responses and the magnetic perturbations prompted by the aforementioned ionospheric currents.

Highlights

Low latitude geomagnetic response associated with intense geomagnetic storms: regional space weather in Mexico

Castellanos-Velazco, C. I., Corona-Romero, P., González-Esparza, J. A., Caccavari-Garza, A. L., Sergeeva, M. A.

- Investigation into space weather dynamics in central Mexico.
- Analysis of disparities between local and planetary geomagnetic responses during geomagnetic storms.
- In-depth study of ionospheric currents as drivers of local geomagnetic fluctuations.

 ccastellanos@igeofisica.unam.mx (C.C. I.);
p.coronaromero@igeofisica.unam.mx (C. P.); americo@igeofisica.unam.mx
(G.J. A.)
ORCID(s): 0000-0001-8818-5318 (C.C. I.); 0000-0002-2573-2967 (C. P.);
0000-0003-4774-1829 (G.J. A.)

Low latitude geomagnetic response associated with intense geomagnetic storms: regional space weather in Mexico

Castellanos-Velazco, C. I.^a, Corona-Romero, P.^b, González-Esparza, J. A.^b, Caccavari-Garza, A. L.^c and Sergeeva, M. A.^{b,**}

^aPrograma de Posgrado en ciencias de la Tierra, Instituto de Geofísica Unidad Michoacán, Universidad Nacional Autónoma de México, , Morelia, 58341, Michoacán, México

^bInvestigadores por México-CONACYT, Servicio de Clima Espacial México, Laboratorio Nacional de Clima Espacial, Instituto de Geofísica Unidad Michoacán, Universidad Nacional Autónoma de México, , Morelia, 58089, Michoacán, México

^cInvestigadores por México-CONACYT, Servicio Magnético, Instituto de Geofísica, Universidad Nacional Autónoma de México, , México city, 04150, México

ARTICLE INFO

Keywords:

Space Weather
Geomagnetic Storms
Regional Response
Ionospheric Currents
Disturbed Dynamo
Disturbed Polar Current 2

ABSTRACT

This study investigates regional space weather phenomena in central Mexico by isolating local geomagnetic responses from their planetary counterparts. Through the analysis of 20 intense geomagnetic storms, we discerned the ionospheric contributions within regional geomagnetic data recorded in central Mexico. Our findings underscore the predominant role of ionospheric disturbances in driving local geomagnetic responses. Notably, the *Disturbed Polar Current Number 2* and the *Disturbed Dynamo Current* emerged as particularly influential factors in regional geomagnetic activity. Importantly, our research establishes that regional geomagnetic responses can be accurately approximated by considering the combined impacts of planetary geomagnetic responses and the magnetic perturbations prompted by the aforementioned ionospheric currents.

1. Introduction

Geomagnetic storms (GS) are significant phenomena within space weather, as they can adversely impact various systems such as communications, navigation, and energy supply [?]. GSs are closely tied to solar activity and primarily involve a temporary weakening of the Earth's magnetic field (EMF), among other effects [?]. These storms arise when solar wind material penetrates the EMF through magnetic reconnection between the interplanetary magnetic field (IMF) and the EMF [? ?].

Geomagnetic storms are typically identified using geomagnetic indices, which quantify their magnitude. Various geomagnetic indices exist, each designed to capture specific aspects of geomagnetic disturbances. In the context of middle and low latitudes, the most commonly used indices are the planetary K index (K_p) and the disturbance storm time index (Dst). These indices are especially effective in regions where the geomagnetic perturbation can be observed on the Earth's magnetic field's horizontal component (H). The K_p index quantifies the maximum variation in H observed at mid-latitudes over three-hour intervals. Similarly, the Dst index represents an hourly average of perturbations in H as measured near the Earth's magnetic equator. These planetary indices, namely K_p and Dst, have regional counterparts that rely on regional data instead of planetary averages [?].

While geomagnetic storms are global phenomena, their manifestation at the regional scale can exhibit variability

across different locations. This variation can be attributed to the Earth's heterogeneity, asymmetries in magnetospheric and ionospheric currents, and the intricate interactions between the magnetosphere and ionosphere in each region. Consequently, geomagnetic latitude, local time, and seasonal variations can influence how a geomagnetic storm unfolds at the regional level. Overlooking these regional factors may lead to uncertainties and misinterpretations when attempting to comprehend and address the potential effects of geomagnetic storm events [? ? ?].

In recent decades, there has been growing interest in studying space weather phenomena within regions characterized by middle and low geomagnetic latitudes. Notably, studies by [? ?], and [?] underscore investigating these phenomena in mid and low latitudes. Taking the case of Mexico, a country situated within these latitudinal ranges, efforts have been made to conduct regional ionospheric and geomagnetic studies [? ? ? ? ? ? ? ?]. However, the systematic study and monitoring of regional space weather formally commenced in 2014 with the initiation of operations by the Mexican Space Weather Service (SCIESMEX) at the Geophysics Institute (IGF) of the National Autonomous University of Mexico (UNAM). Subsequently, by 2016, a significant expansion of infrastructure and technologies dedicated to studying and monitoring regional space weather was achieved by establishing the Mexican Space Weather National Laboratory (LANCE) at IGF-UNAM [?].

Through collaborative efforts and resource sharing, the SCIESMEX/LANCE collaboration has identified the potential role of ionospheric disturbances in driving regional geomagnetic response during geomagnetic storm periods [see ? ? ? ?]. This finding aligns with other studies conducted in mid and low latitudes, as it is known that for these latitudinal

*Corresponding author

 ccastellanos@geofisica.unam.mx (C.C. I.);

p.coronaromero@geofisica.unam.mx (P. P.); americoo@geofisica.unam.mx (G.J. A.)

ORCID(s): 0000-0001-8818-5318 (C.C. I.); 0000-0002-2573-2967 (C. P.); 0000-0003-4774-1829 (G.J. A.)

ranges, two primary sources of geomagnetic fluctuations driven by ionospheric currents exist: the *disturbed polar current number 2* (DP2) [? ? ?], and the *disturbed dynamo current* (Ddyn) [?].

On one hand, the DP2 current is linked to electric fields induced during the magnetic reconnection between the interplanetary magnetic field and the EMF. These electric fields are then transported along the Birkeland currents [? ?], eventually reaching high ionospheric latitudes where they give rise to a pattern of two ionospheric convective twin cells known as DP2 currents. The charged particles within these cells are carried by the centrifugal and curvature effects of the EMF, resulting in the induction of a polarized electric field [? ? ? ? ?]. During the main phase of a geomagnetic storm, this polarized electric field, coupled with the DP2 current, can extend beyond high latitudes, encompassing mid and even low latitudes [? ? ?].

On the other hand, Ddyn currents represent amplifications of the polar ionospheric currents due to the precipitation of energetic particles during the main phase of a geomagnetic storm. The resulting Joule heating in the thermosphere generates the circulation of neutral winds and charged particles in the equatorward direction. The Coriolis force induces a westward shift in the direction of these polar-equatorial flows at mid and low latitudes [? ? ?]. Equatorward Pedersen currents are induced in this process, leading to the accumulation of charged particles along the dip equator. This accumulation, in turn, triggers the generation of poleward-directed electric fields and a second Pedersen current in the same direction but opposing the first one. Consequently, Hall currents are driven eastward at mid-latitudes (approximately 45°), and these currents are interrupted at termination points [?]. This sequence of events results in currents diverging and closing at adjacent latitudes, forming the distinct vortex-shaped currents known as *Disturbed dynamo currents*.

Given that the Ddyn and DP2 ionospheric currents possess the potential to influence the geomagnetic response in mid and low latitudes, it raises the question of whether these ionospheric mechanisms are responsible for linking regional geomagnetic response to local ionospheric perturbations in central Mexico. This inquiry constitutes the primary motivation for our study. Throughout this work, we first seek to identify disparities between regional and planetary geomagnetic activities to isolate regional geomagnetic responses during geomagnetic storms. With this regional response isolated, we search for evidence of Ddyn and DP2 mechanisms as sources of such regional geomagnetic response. Our approach involves identifying their respective signatures within magnetic records. Subsequently, we validate our findings by comparing planetary and regional geomagnetic activity indices, culminating in a discussion of our concluding remarks.

In the next section, we present the methodology employed to accomplish these objectives and provide further insights into the specifics of our investigation.

2. Methodology

2.1. Local geomagnetic response

We analyzed 20 geomagnetic storm (GS) events to identify regional geomagnetic responses. These events spanned from 2003 to 2018, encompassing the descending phase of solar cycle 23 and a significant portion of solar cycle 24. The observations were obtained from the Geomagnetic Observatory of Teoloyucan (TEO), located at 27.84°N and 28.41°W. TEO is operated by the Magnetic Service of the Geophysics Institute at the National and Autonomous University of Mexico. Specifically, we selected events with a local K index (K_{TEO}) above 6+ and ΔH_{TEO} (the regional equivalent of the Dst index) below -120 nT. Table 1 provides details of all the analyzed events.

We hypothesize that the significant discrepancies observed between regional and planetary geomagnetic indices are due to local geomagnetic responses. To explore this, we directly compared Dst with ΔH_{TEO} for the analyzed events. The dispersion plot in Figure 1 illustrates this comparison, plotting regional response on the vertical axis against its planetary counterpart on the horizontal axis. The plot reveals two distinct trends in data distribution:

1. For events with $Dst \geq -100$ nT, the data points closely adhere to the identity line (solid black line).
2. For events with $Dst < -100$ nT (green-shadowed region), the data points deviate from the identity line.

These trends align with correlation indices, yielding $R^2 = 0.77$ for the former and $R^2 = 0.42$ for the latter.

In light of the differences observed between regional and planetary geomagnetic indices during our analysis of these events, local mechanisms (likely ionospheric) may contribute to the deviations in the regional geomagnetic field from its planetary counterpart. Consequently, our next objective is to identify signatures within the regional geomagnetic records that can be attributed to the magnetic contributions of these ionospheric mechanisms [? ? ? ?]. We will now proceed with the investigation of these mechanisms.

2.2. Geomagnetic signatures of local ionospheric currents

The local values of the Earth's magnetic field (EMF) result from the combined contributions of various sources [? ? ? ?]. Specifically, for the horizontal component (H) of the local EMF, it can be expressed as follows:

$$H = B_{SQ} + H_0 + D_M + D_I, \quad (1)$$

Here, B_{SQ} represents the diurnal variation derived from local quiet days [?], while H_0 captures the day-to-day variations [?]. The final two terms, D_M and D_I , correspond to irregular magnetic variations associated with geomagnetic activity [? ?]. Specifically, D_M accounts for contributions from planetary-scale magnetospheric currents, while D_I is linked to magnetic perturbations caused by ionospheric disturbances. Notably, for mid and low latitudes, D_M can be

Table 1

Study cases: Event number, GS main phase beginning date, minimum (maximum) values reached during the events for Dst(K_p) and $\Delta H_{TEO}(K_{TEO})$ geomagnetic indices, respectively.

Event #	Beginning of main phase	^a Dst minimum [nT]	^b ΔH minimum [nT]	^a K_p maximum	^b K_{TEO} maximum
1	2003/05/29	-144	-190	8+	9
2	2003/10/14	-85	-126	7+	7-
3	2003/11/20	-422	-441	9-	9
4	2004/07/22	-170	-167	9-	8+
5	2004/08/30	-129	-154	7	7-
6	2004/11/08	-374	-398	9-	9
7	2005/05/15	-247	-206	8+	7
8	2005/06/12	-106	-120	7+	6+
9	2005/08/24	-184	-138	9-	9-
10	2005/08/31	-122	-125	7	6+
11	2006/08/19	-79	-131	6	7-
12	2006/12/14	-162	-247	8+	9
13	2015/03/15	-222	-282	8	8-
14	2015/10/07	-124	-143	7+	7+
15	2015/12/20	-155	-189	7-	7
16	2016/03/06	-98	-120	6	7
17	2016/10/13	-104	-128	6+	6+
18	2017/05/27	-125	145	7	8
19	2017/09/07	-124	-170	8+	8+
20	2018/09/25	-175	-176	7+	7-

Comments for the Table.

^a Dst and K_p were obtained from the International Service of Geomagnetic Indices (ISGI).

^b Regional geomagnetic indices ΔH_{TEO} and K_{TEO} were computed by the Space Weather National Laboratory, using TEO geomagnetic records.

approximated by $Dst \cdot \cos(\lambda)$, where λ is the geomagnetic latitude [?]. This approximation simplifies Equation 1 to:

$$D_I \approx H - (B_{SQ} + H_0 + Dst \cdot \cos(\lambda)). \quad (2)$$

Furthermore, D_I can be decomposed into individual components as follows:

$$D_I = DP2 + Ddyn + D_{others}, \quad (3)$$

Here, D_{others} refers to ionospheric perturbations distinct from $DP2$ and $Ddyn$.

To effectively isolate the magnetic signatures attributed to $DP2$ and $Ddyn$ in Equations (2) and (3), we will employ frequency filters to analyze D_I [?]. These filters will be designed based on the frequency range (periods) associated with magnetic fluctuations induced by each current in the local EMF. Specifically, it is established that the magnetic fluctuations induced by $Ddyn$ exhibit primary periods of approximately 24 h. In contrast, the oscillation periods of fluctuations induced by $DP2$ are equal to or less than 4 h [? ?]. As a result, the filters employed will be a pass-band filter for $DP2$ and a high-pass filter for $Ddyn$ [? ?].

3. Analysis and results

3.1. Local ionospheric disturbances and induced magnetic fluctuations

In this section, we present our analysis process through analyzing event 13. The panel (a) of Figure 2 shows the profiles of Dst (black) and ΔH (green) indices during the GS associated with event 13 (see Table 1). In the panel, we observe that both indices are *quiet* up to the start of the GS's main phase, signed out by a vertical dotted line. The main phase lasts approximately one day, reaching a minimum of $Dst \sim -300$ nT, whereas the recovering phase extends almost three days.

In the panel (b) of Figure 2, we appreciate the resulting profile of D_I (Equation (2)), which we computed using the TEO's registers and the Dst reported data. Subsequently, we construct a power spectrum for our computed profile of D_I , which we show in panel (d) of Figure 2. In the power spectrum, we highlight, by a yellow shadowing, the range of periods(frequencies) consistent with $DP2$ and $Ddyn$. In the panel, we identify $Ddyn$'s range by setting the main period and searching potency peaks within the range of possible harmonics. It is important to remark that, because our study cases might be potentially different from each other, the filtering ranges might vary slightly from case to case.

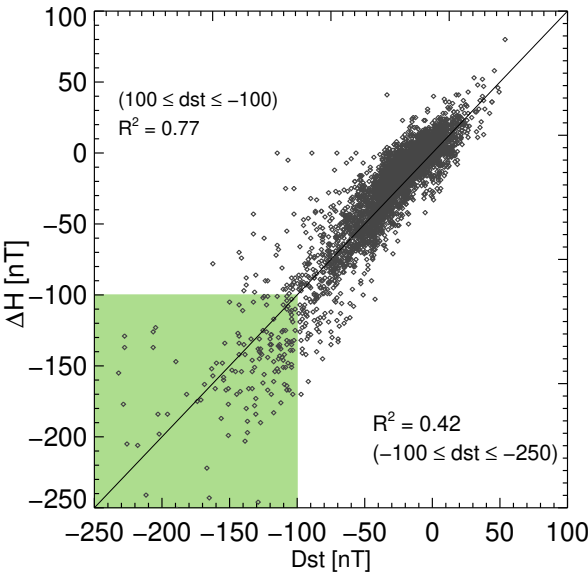


Figure 1: Dispersion plot of ΔH (vertical axis) with respect to Dst (horizontal axis) for all GS events. The green region represents a -100 nT threshold in which it was computed a second R^2 .

In Figure 2(c) we present the profiles of the induced magnetic perturbations caused by $DP2$ (solid red line) and $Ddyn$ (solid black line). These profiles are constructed departing from the frequencies identified through the filtering process commented on in the previous paragraph. We note that the enhancements of the induced effects of $Ddyn$ and $DP2$ simultaneously occur with an increase in the total electron content over central Mexico, as the panel (e) of Figure 2 shows.

We applied the procedure presented in this section to all our study cases. The Figures 6 and 7 in the Appendix show the computed D_I and the resulting profiles of $DP2$ and $Ddyn$, for each event in Table 1. We remark on the uniqueness of each event, which is clear in the D_I profiles and its associated magnetic perturbations induced by $DP2$ and $Ddyn$ currents.

From Figures 6 and 7, we note that generally, the amplitude of the magnetic oscillations induced by $Ddyn$ are more intense than those induced by $DP2$. This suggests that, in most cases, $Ddyn$'s induced magnetic effects are dominant on the local EMF. Although there are events for which both effects show similar intensities. We think of two possibilities to explain that: The first is the process that triggers the GS itself, *i.e.* the solar activity event, and its magnetic reconnection with the EMF. This may affect the evolution of the ionospheric response, directly modifying the evolution of $DP2$ and $Ddyn$ currents. Secondly, we have to consider that our data is sampled in hourly resolution. In this case, data sampling represents an important limitation since $DP2$ magnetic fluctuations, as mentioned in [?], may have periods of less than an hour or even of tens of minutes. In this scenario, we possibly missed part of $DP2$ fluctuations during our analysis. This could be solved, in principle, by

using $Sym - H$ index rather than Dst , a task in which exploration we consider our future work.

3.2. Validation of DP2 and Ddyn magnetic signatures

In Section 2.1, we identified substantial differences between planetary and regional geomagnetic activity, attributing these distinctions to regional geomagnetic responses. In Section 3.1, we pinpointed the tentative geomagnetic mechanisms behind these responses—namely, the $Ddyn$ and $DP2$ ionospheric currents—by employing a process of frequency filtering. Furthermore, we established that these effects correlate systematically with local Total Electron Content (TEC) perturbations. To validate these findings, a multi-step approach is necessary.

Initially, we approximate the regional geomagnetic index ΔH by defining it as follows:

$$\Delta H = H - (B_{SQ} + H_0), \quad (4)$$

Using Equations (2), (3), and (4), we derive:

$$\Delta H \approx Dst \cos(\lambda) + DP2 + Ddyn. \quad (5)$$

To simplify, we denote Dst_λ as the combined effect of $Dst \cos(\lambda)$, $DP2$, and $Ddyn$. This leads to our first validation step, confirming whether the computed Dst_λ approximates ΔH . Additionally, we employ Dst_λ and the values of K_p to approximate the local K value.

Figure 3 portrays the validation process applied to event 13. The top panel juxtaposes profiles of ΔH (black), Dst (green), and Dst_λ (red). It is evident that Dst_λ consistently tracks closer to ΔH than Dst , holding true during the main and recovery phases of the geomagnetic storm (GS). The bottom panel reveals that the values of planetary (green) and local (black) K differ. However, when Dst_λ is combined with K_p values using uncertainty bars, the local K profile generally falls within this range.

To validate comprehensively, this process is applied to all studied cases. Figures 8 and 9 showcase the results. Consistently, Dst_λ approximates ΔH , and K_p with the effects of Dst_λ encapsulates regional K values.

Additionally, a quantitative assessment is conducted. The average absolute differences between $\Delta H - Dst$ and $\Delta H - Dst_\lambda$ pairs across the study cases are computed. As displayed in Figure 4, the histogram illustrates the average differences between $\Delta H - Dst$ (blue bars) and $\Delta H - Dst_\lambda$ (red bars). Notably, the average difference associated with Dst_λ consistently outperforms that of Dst , implying the relevance of magnetic perturbations corresponding to $DP2$ and $Ddyn$ for regional geomagnetic responses.

The final step involves remaking the dispersion plot from Figure 1, employing Dst_λ data instead of Dst . The resulting Figure 5 depicts data points (open diamonds) closely following the identity (solid black line), in contrast with Figure 1. Moreover, R^2 improves from 0.77 to 0.86 for $Dst \geq -100$ nT, and for $Dst < -100$ nT, R^2 rises to 0.75, a significant increase from the original Dst value ($R^2 = 0.42$).

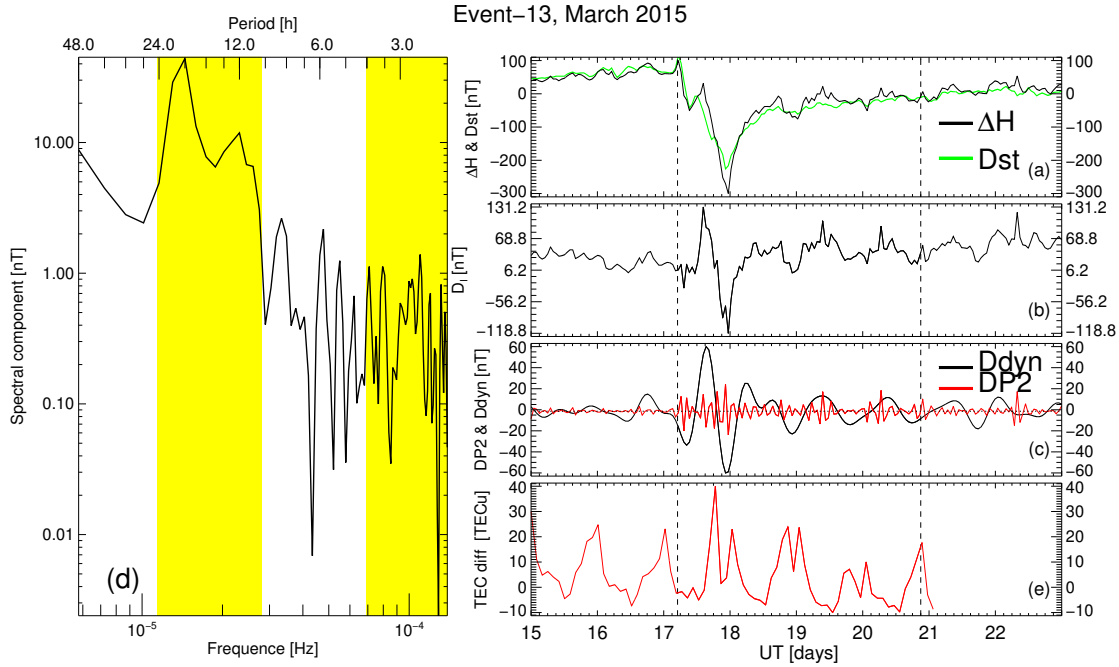


Figure 2: Analysis of study case 13. Panel (a): Dst (black) and ΔH (green). Panel (b): computed value of D_I . Panel (c): Reconstructed profiles of the induced geomagnetic effects of D_{dyn} (black line) and DP_2 (red line). Panel (d): Power spectrum of D_I . Panel (e): Measured total electron content (TEC) over the center of Mexico. Dotted vertical lines mark out GS's start (left) and end (right). Yellow shadowing regions in panel (d) highlight the bandwidths associated with D_{dyn} (25h - 10 h) and DP_2 (less than 4.5 h) filters.

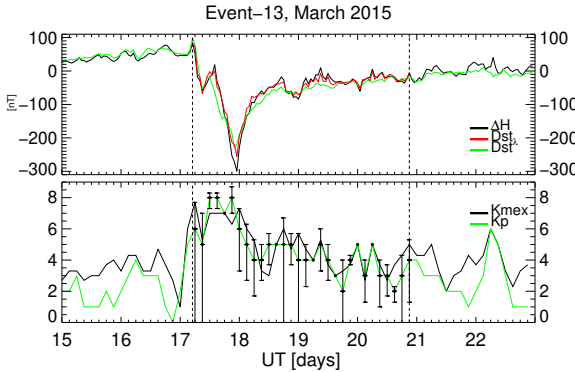


Figure 3: Approximation of ΔH (top) and local K (bottom) geomagnetic indices. The green solid lines represent planetary indices and black solid lines represents local geomagnetic indices. The approximated ΔH index is represented by the red line while the error bars represent an approximation range for K_{mex} index.

Our validation process proved that the magnetic perturbations tentatively induced by DP_2 and D_{dyn} ionospheric currents, when combined with planetary indices, allowed to qualitatively approximate the regional geomagnetic activity. We also proved that regional geomagnetic response, as registered by ΔH , can be quantitatively expressed by the planetary response (Dst) combined with the geomagnetic effects of the already commented ionospheric currents. Finally, when including the magnetic effects induced by

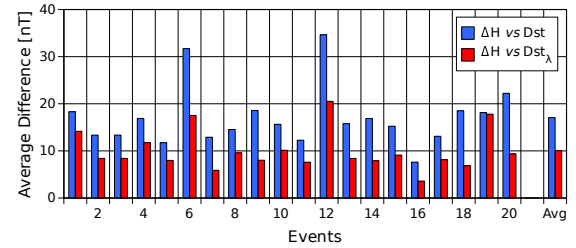


Figure 4: Average error (Top) measured in nT between ΔH vs Dst and ΔH vs Dst_λ . Error difference (bottom) between the two cases above.

DP_2 and D_{dyn} into the planetary response, the dispersion between regional and planetary data substantially decreased.

Through this validation process, we successfully demonstrate that the magnetic perturbations potentially induced by DP_2 and D_{dyn} ionospheric currents, when combined with planetary indices, allow for qualitative and quantitative approximations of regional geomagnetic activity. Furthermore, the disparity between regional and planetary data is substantially reduced by integrating the magnetic effects resulting from DP_2 and D_{dyn} into the planetary response.

4. Concluding remarks

In this work, we studied the regional manifestations of space weather. We focused on the differences between

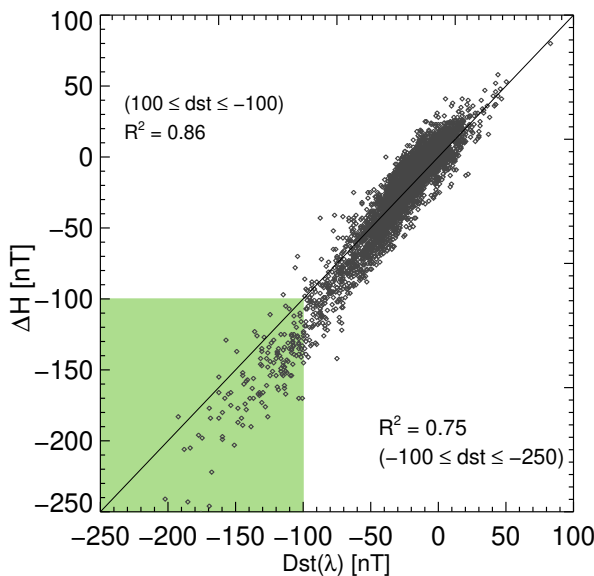


Figure 5: Dispersion plot of ΔH (vertical axis) with respect to Dst_λ (horizontal axis) for all GS events. The green region represents a -100 nT threshold in which it was computed a second R^2 .

planetary and local geomagnetic responses during periods of strong geomagnetic storms (GS) at the center of Mexico. We also investigated the possible sources for such differences in the geomagnetic response. We used the geomagnetic registers from the Teoloyucan Magnetic Observatory (TEO), located north of Mexico City. We also use data sets from the Dst and K_p planetary indices, the regional geomagnetic index ΔH , and the total electron content delivered by the Mexican Space Weather National Laboratory.

We selected 20 GS as study cases for this work (see Table 1). For all our study cases, we identified evidence of relevant regional geomagnetic response through a dispersion plot (see Figure 1). In this regard, we found that in the range of $Dst < -100$ nT, there is a tendency for the regional geomagnetic index to deviate from the planetary one. We assumed this as evidence for a regional geomagnetic response.

Subsequently, we isolated the geomagnetic effects due to ionospheric processes (D_I) from the regional (TEO) geomagnetic registers. Next, we applied filters on D_I to identify the magnetic perturbations consistent with those induced by $Ddyn$ and $DP2$ currents. We also verified that intensifying the resulting $Ddyn$ and $DP2$ profiles simultaneously occurred during TEC perturbations (see discussion of Figure 2). Consequently, we could reconstruct the regional geomagnetic response consistent with those induced by $Ddyn$ and $DP2$ currents.

Afterward, we validate our computed geomagnetic contribution due to $Ddyn$ and $DP2$ currents. First, we approximate the regional K and ΔH indices by combining the planetary K_p and Dst indices with the regional geomagnetic effects of $Ddyn$ and $DP2$. Secondly, we computed the differences between ΔH and Dst with and without the regional

ionospheric effects. Finally, we analyzed the dispersion between ΔH and Dst combined with the effects of $Ddyn$ and $DP2$. For all the cases, we found that regional geomagnetic response is qualitatively and quantitatively approximated by the geomagnetic planetary response combined with the geomagnetic perturbations induced by the $Ddyn$ and $DP2$ ionospheric currents.

Finally, in this work, we focus on regional space weather. We identified evidence of a significantly different regional geomagnetic response from its planetary counterpart. We investigated $Ddyn$ and $DP2$ ionospheric currents as the mechanisms for such a regional response. As a result, we were able to isolate the magnetic perturbations associated with those ionospheric currents. Combining these perturbations with the planetary response could approximate the regional geomagnetic response.

CRediT authorship contribution statement

Castellanos-Velazco, C. I.: Methodology, Conceptualization, Data analysis, Software, Writing - Original Draft. **Corona-Romero, P.:** Conceptualization, Methodology, Software, Writing - Review & Editing. **González-Esparza, J. A.:** Data revision, Review & Editing. **Caccavari-Garza, A. L.:** Regional magnetic data, Review & Editing. **Sergeeva, M. A.:** Local ionospheric data, Review & Editing.

Declaration of competing interest

The authors declare that they have no known competing financial interests or personal relationships that could have appeared to influence the work reported in this paper.

Data Availability

Data will be made available on request.

Acknowledgments

P. Corona-Romero is grateful for Investigadores por México-CONAHCYT (CONAHCYT Research Fellow) project 1045 Space Weather Service, financed by “Consejo Nacional de Ciencia y Tecnología” (CONAHCYT), which partially supported this work. C.I. Castellanos-Velazco is grateful for “La Beca de Posgrado en México” granted by CONAHCYT. LANCE acknowledges partial financial support from CONAHACyT-AEM grant 2017-01-292684, CONAHACyT LN-315829, and PAPIIT IN116023.

This work used data from the Teoloyucan Magnetic Observatory operated by the Magnetic Service of the Geophysics Institute at the National and Autonomous University of Mexico (UNAM). Total electron content (TEC) and the geomagnetic indices ΔH and K , the regional counterparts of Dst and K_p indices, respectively, are produced by the Mexican Space Weather National Laboratory (LANCE), Geophysics Institute at National and Autonomous University of Mexico (UNAM).

The results presented in this paper rely on K_p and Dst geomagnetic indices calculated by the Helmholtz-Zentrum Potsdam Deutsches GeoForschungsZentrum Adolf-Schmidt-Observatorium and the World Data Center for Geomagnetism, Kyoto, respectively, from data collected at magnetic observatories. We thank the involved national institutes, the INTERMAGNET network and ISGI.

All authors have seen and approved the final version of the manuscript.

5. Appendix

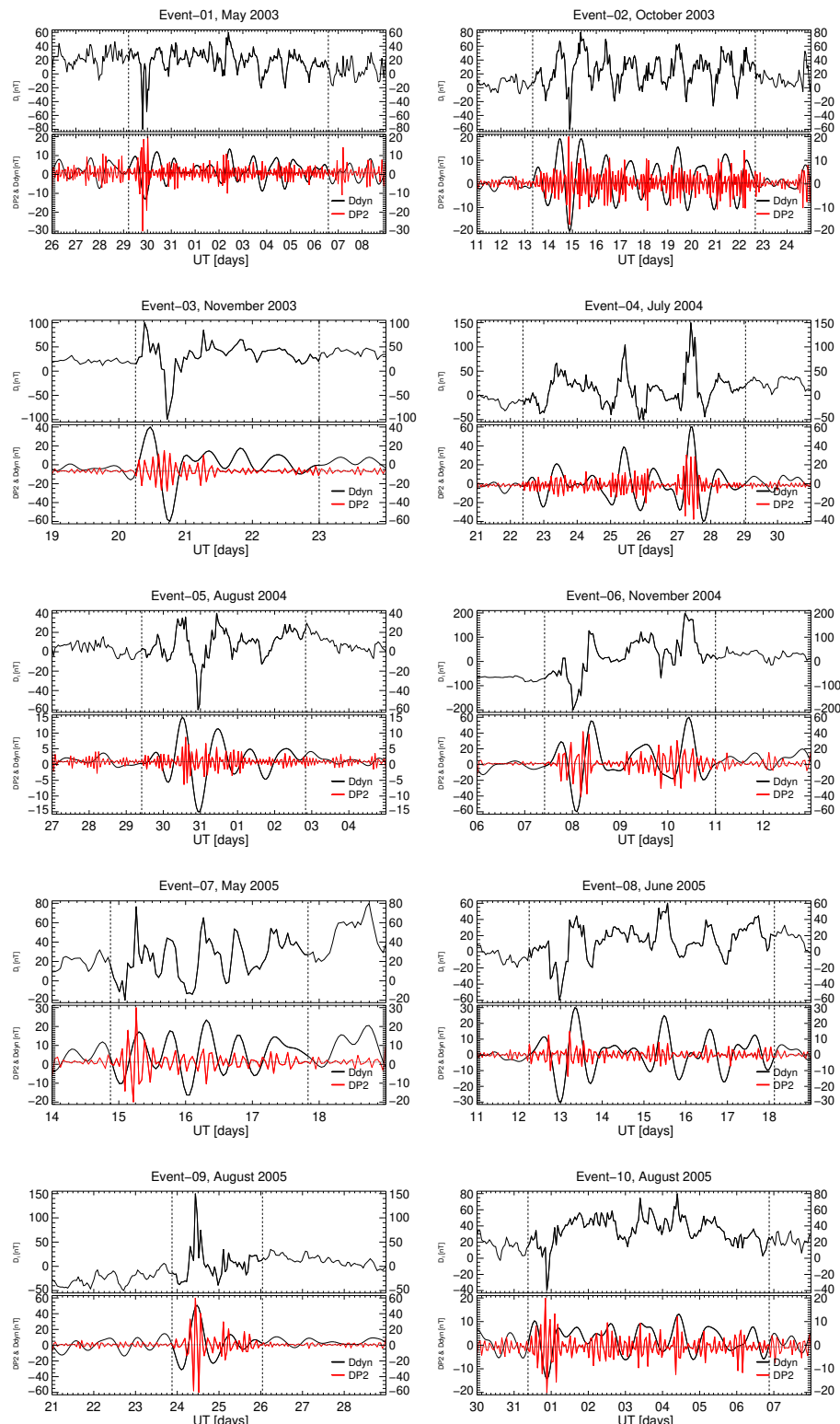


Figure 6: Ionospheric Magnetic Disturbance contribution (top panels) and the isolated Ddyn and DP2 geomagnetic contribution (bottom panels).

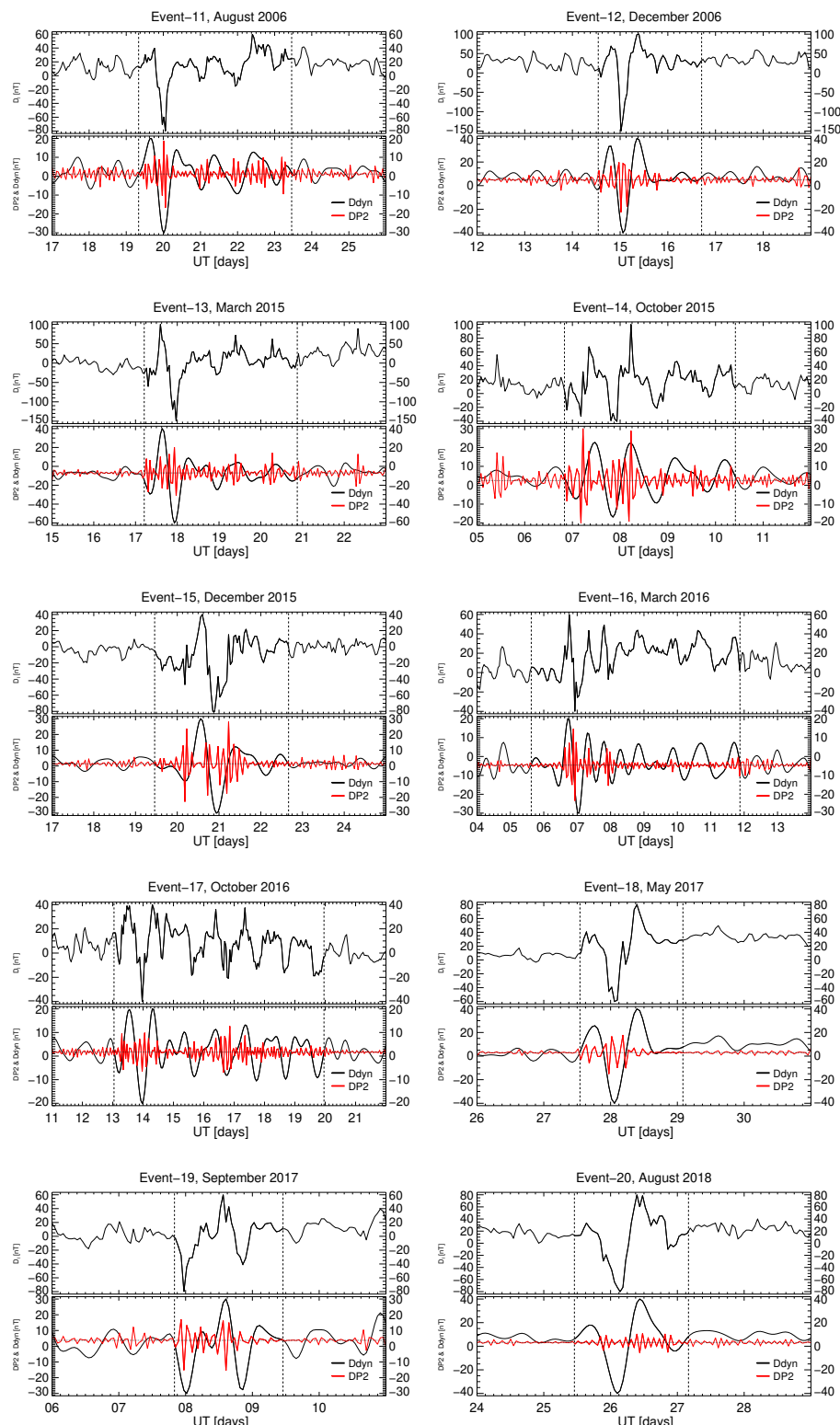


Figure 7: Ionospheric Magnetic Disturbance contribution (top panels) and the isolated D_{dyn} and DP_2 geomagnetic contribution (bottom panels).

Geomagnetic local response associated with geomagnetic storms

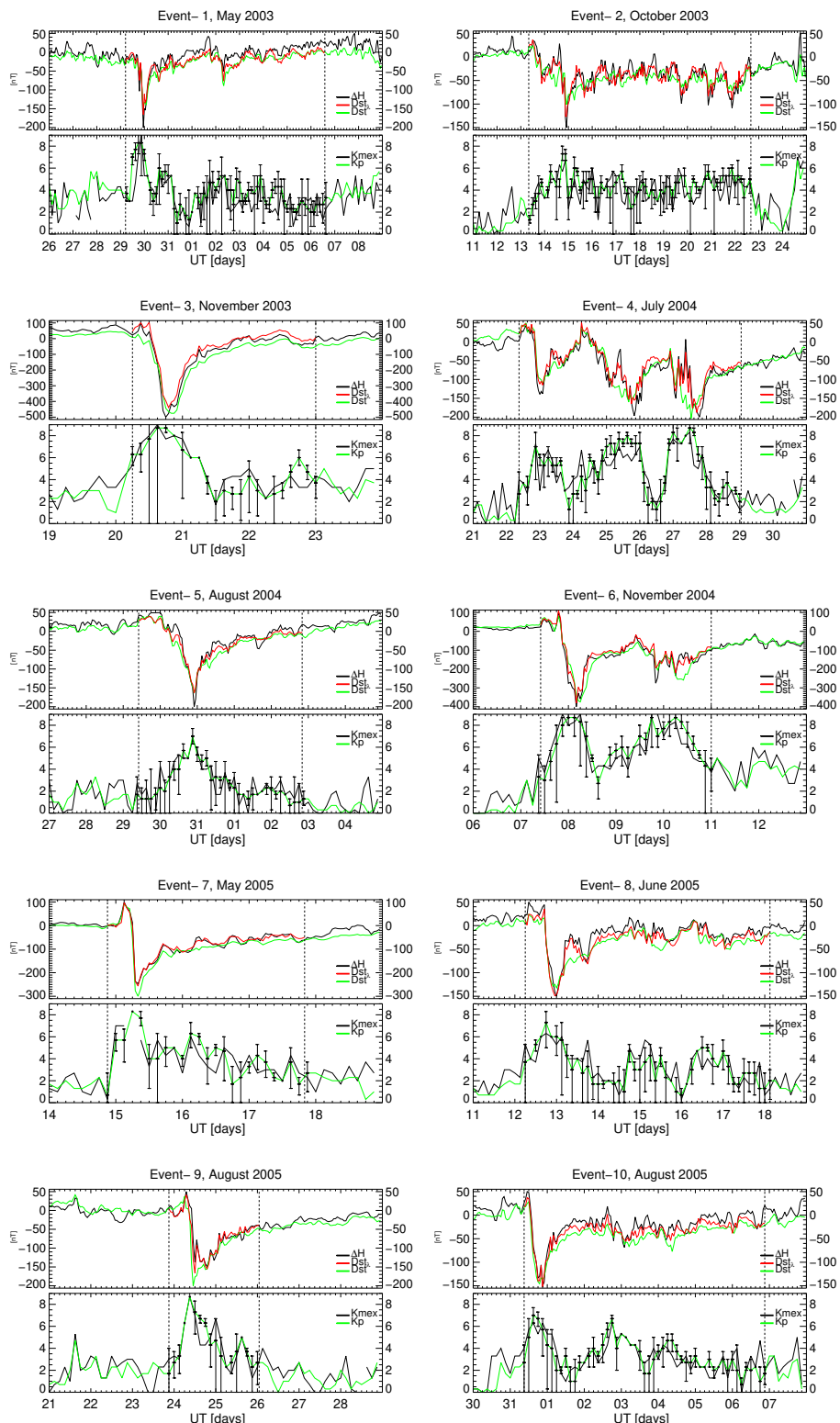


Figure 8: Top: Approximation of ΔH (red line). Bottom: Approximation of K local with a ΔK affection range (error bars).

Geomagnetic local response associated with geomagnetic storms

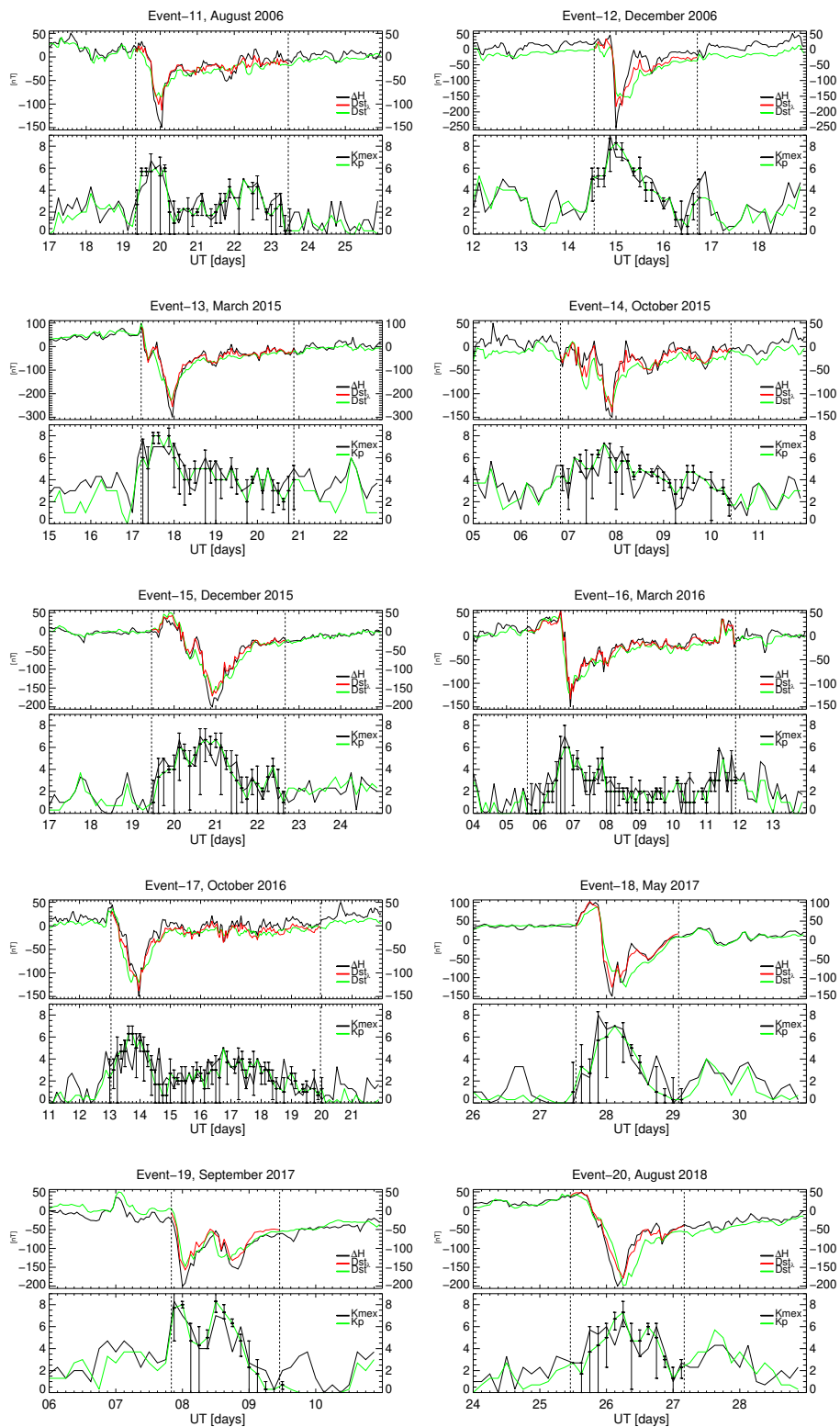


Figure 9: Top: Approximation of ΔH (red line). Bottom: Approximation of K local with a ΔK affection range (error bars).